CHAPTER 10

NANOCOMPOSITES AS HIGH EFFICIENCY THERMOELECTRIC MATERIALS

Suraj Joottu Thiagarajan, Wei Wang and Ronggui Yang*

Department of Mechanical Engineering, University of Colorado, Boulder, CO 80309, USA
**Email: Ronggui.Yang@colorado.edu*

The phenomenon of thermoelectricity provides a means of directly converting electricity to a temperature gradient and vice versa, using the electrical carriers, electrons and holes, in the solid state devices as the working fluids with no moving parts. This offers many distinguished characteristics such as that they are environmentally friendly, quiet, compact and scalable. However the inherent low efficiency of thermoelectric devices based on conventional materials has restricted their use only to niche applications, such as power generators for space exploration and temperature control for some laboratory instruments. In the last 15 years, significant progress has been made in developing higher efficiency thermoelectric materials and this has led to a renewed interest in the field of thermoelectric energy conversion. Central to this advancement is the recognition that nanostructured materials make it possible to effectively decouple the Seebeck coefficient, electrical conductivity and thermal conductivity, all of which are intimately connected in conventional materials, and vary each of these somewhat independently. This review describes some recent developments in the field with emphasis on the development of bulk nanostructured materials, i.e. nanocomposites. After a brief review of the theoretical foundation of high efficiency thermoelectric nanocomposites and the synthesis methods for nanocomposites, we review the different classes of materials recently developed for various applications in different operating temperature ranges.

1. Introduction to Thermoelectricity

With the rising demand for energy, the impending energy scarcity and problems of global warming due to fossil fuels, it is incumbent on us to develop new and more efficient ways of utilizing energy. This has motivated the development of cleaner and renewable energy technologies such as solar photovoltaics, wind power, tidal power, among others.

Thermoelectric phenomenon is the direct conversion between electric and thermal energy, and offers a convenient means for heating and cooling materials and direct electricity generation from thermal sources. The most familiar example is a thermocouple, where the open circuit voltage of a junction between two dissimilar conductors is determined by the temperature of the junction. If instead of open-circuit operation, the thermocouple is allowed to do work across an electrical load, then the device operates as a thermoelectric power generator (Fig. 1(a)). Alternatively, if the load is replaced with an electrical power source to reverse the current flow, then the device operates as a refrigerator or heat pump (Fig. 1(b)).

Compared to traditional refrigerators and heat engines, thermoelectric energy converters have the advantages of simplicity, reliability, no vibrations, and scalability. Furthermore, because they use no refrigerants or working fluids, thermoelectric devices may be expected to have negligible direct emissions of greenhouse gases over their lifetime, likely reducing their contribution to global warming compared to conventional technologies. Due to this combination of desirable qualities, they are ideal for applications such as household refrigeration and recovery of heat energy in automobile and industrial exhaust gas that is otherwise dumped to the atmosphere, or integrated solar-thermoelectric systems for harnessing the thermal energy in the solar spectrum. Despite the possibility of such attractive applications, however, thermoelectric technology is not widespread due to the fact that the efficiency of devices made of conventional thermoelectric materials is very low. Thus, it has been limited to such niche applications as radioisotope thermoelectric power generators (RTGs) for space probes, heating or cooling car seats in luxury cars, and temperature control of some laboratory instruments.

The efficiency of heat to electrical energy conversion in a thermoelectric generator, as shown in Fig. 1(a), depends on many parameters, including the material properties Seebeck coefficient S, electrical conductivity σ and thermal conductivity κ; the (absolute) temperatures of the hot side T_H and the cold side T_C, and the load resistance. The thermal conductivity of a typical material has contributions of both electrons and phonons, denoted as κ_e and κ_p, respectively. Joule heating and heat conduction inside the device cause irreversible energy losses, leading to lower efficiency. The efficiency can be calculated by considering it as a thermodynamic heat engine, and taking into account the different energy losses. Under optimized load conditions, assuming that the material properties are constant within each thermoelectric leg, and that the contact resistances are negligible compared to the total resistance in the arms, the efficiency η of power generation is given by [1, 2]

$$\eta = \frac{T_H - T_C}{T_H} \cdot \frac{\sqrt{Z\bar{T}+1}-1}{\sqrt{Z\bar{T}+1}+T_C/T_H} \tag{1}$$

where $\bar{T}$ is the mean temperature in each arm.

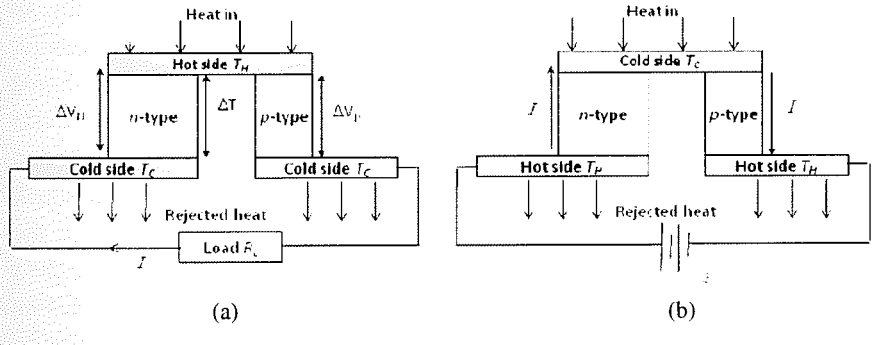

Figure 1. A thermoelectric couple with semiconducting n- and p-type arms configured for (a) power generation and (b) refrigeration.

If the device is configured for refrigeration, then the coefficient of performance (COP) can be obtained similarly as,

$$COP = \frac{T_C\left[\sqrt{Z\bar{T}+1} - \frac{T_H}{T_C}\right]}{(T_H - T_C)\left[\sqrt{Z\bar{T}+1}+1\right]} \quad (2)$$

In both of the above equations which quantify the maximum achievable performance of thermoelectric power generators and refrigerators, the materials properties S, σ, and κ appear in the combination $S^2\sigma/\kappa$, making it convenient to define this quantity as the *thermoelectric figure of merit* of the material. This provides a means for the assessment of a material for its suitability for the use in a thermoelectric device. The figure of merit can be defined non-dimensionally as

$$ZT = \frac{S^2\sigma}{\kappa}T \quad (3)$$

A good thermoelectric material is the one with a high Seebeck coefficient, a high electrical conductivity, and a low thermal conductivity. As all the three properties are interconnected, it has proved impossible to raise the value of the ZT to much over 1 in bulk materials till recently. The best thermoelectric materials are found in heavily doped semiconductors. Insulators have poor electrical conductivity and metals have low Seebeck coefficient. In semiconductors, the phonon contribution to the thermal conductivity can be reduced without much reduction in electrical conductivity. A proven approach to reduce the phonon thermal conductivity is through alloying proposed in later 1950's [3]. The mass difference scattering in an alloy reduces the lattice (phonon) thermal conductivity significantly without much degradation to the electrical conductivity. Figure 2 shows the figure of merit vs. temperature of some of the common bulk thermoelectric materials, in their respective operating temperatures. Usually we could categorize the

thermoelectric materials according to the temperature range where their peak ZT occurs as low temperature materials (200K-400K), mediate temperature materials (400K-800K), and high temperature materials (above 800K). For example, the commercially available thermoelectric materials for room temperature operation are from the $(Bi_{1-x}Sb_x)_2(Se_{1-y}Te_y)_3$ alloy family that reach ZT~1 around room temperature. This class of materials currently dominates in temperature control and thermal management applications. High temperature materials such as silicon germanium alloys are heavily investigated and used for space exploration. Medium temperature range thermoelectric materials could have significant impacts on waste heat recovery and solar thermal utilization.

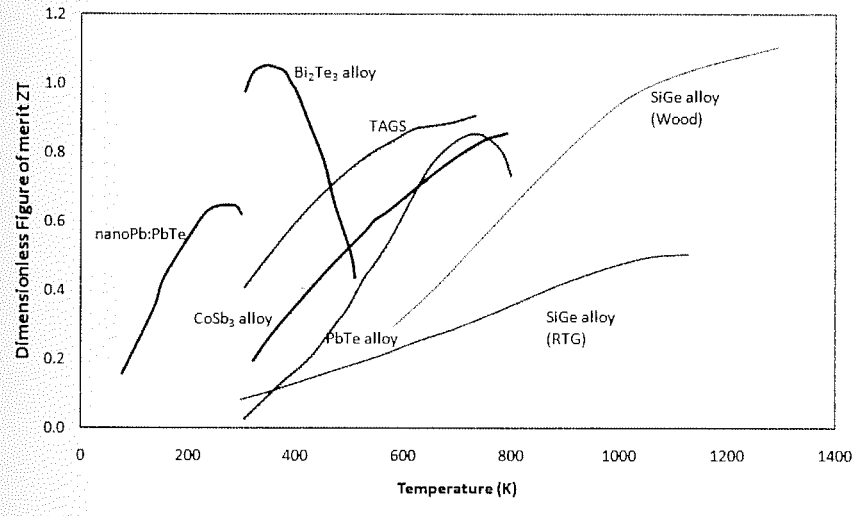

Figure 2. Dimensionless figure of merit ZT at different temperature ranges of conventional materials.

Figure 3 shows that the efficiency of thermoelectric power generation with T_h/T_c=2.5 is about 13% (T_H≈480°C, T_C≈30°C). This situation might apply to waste heat scavenging from automobile exhaust. However, to be able to achieve efficiencies that are competitive with conventional technologies for power generation and refrigeration, and thus to achieve widespread utilization of thermoelectrics, we need to

develop materials with ZT of about 3 or higher, that can be manufactured in large quantities inexpensively. If thermoelectric materials could have a ZT=3, the efficiency of the same waste heat scavenging application almost doubles to 24%. This vastly improved efficiency could open up many more potential applications for thermoelectric energy conversion by lowering the operating cost, although the important issue of the capital cost of the materials still needs to be addressed.

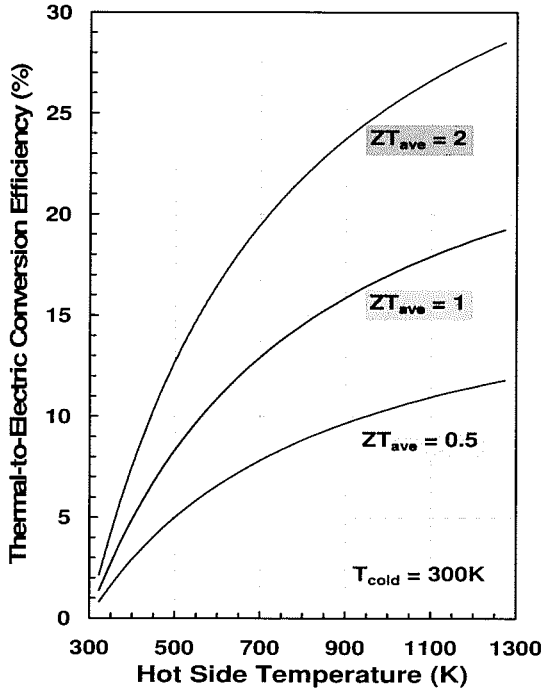

Figure 3. Efficiency of power generation vs. hot side temperature using a thermoelectric generator for materials of various ZTs. The cold side is kept at room temperature.

Figure 4 shows the historic progress of high efficiency thermoelectric materials. The maximum ZT has stayed stagnant at around 1 for all temperature range over 50 years since the important advancements using alloying approach. In the 1990s, two parallel approaches were proposed for the enhancement of the ZT of thermoelectric materials. We have witnessed heightened interests in

thermoelectrics due to the significant ZT improvements published around year 2000. The first of these approaches is based on new categories of advanced bulk materials [4-6], with crystal structures that contain weakly bound atoms or molecules with large vibrational amplitudes (called ratters) at partially filled structural sites acting as effective phonon scatterers. The notion of *phonon glass-electron crystal* (PGEC) enunciated by Glen Slack [7] has been useful in guiding the efforts in this direction. Material systems, such as skutterudites (e.g., $CoSb_3$) [8-10], clathrates (e.g., $Ba_8Ga_{16}Ge_{30}$) [11-13] and Zintl phases [14] belong to this category.

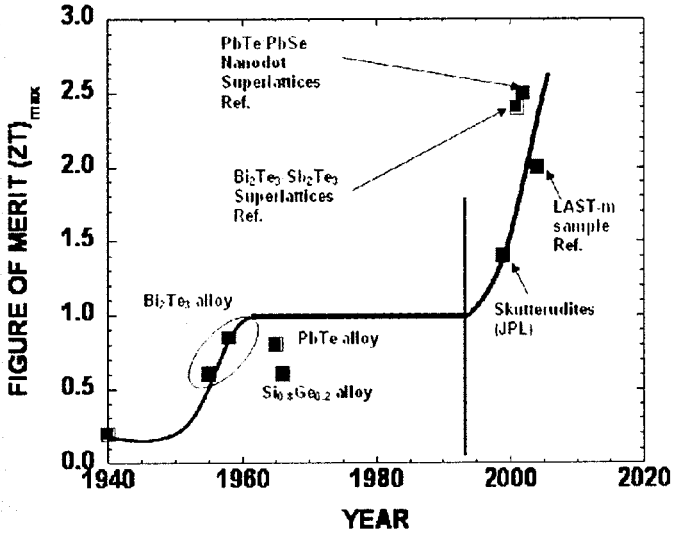

Figure 4. Dimensionless figure of merit of some of the recent materials showing the quantum size effects and low thermal conductivity due to selective phonon scattering.

The second approach is using low-dimensional materials (such as quantum well superlattices, quantum wires and quantum dots) [15, 16] that would result in an enhancement of the ZT by two mechanisms: (i) nanoscale features that introduce quantum confinement effects in the material lead to an enhancement of the power factor $S^2\sigma$, and (ii) the use of the numerous interfaces in the nanostructures that scatter phonons more than the electrons, based on the difference in their respective

scattering lengths, and thus reducing the thermal conductivity without adversely affecting the electrical conductivity as much [17, 18].

The first phase of the investigation of low-dimensional thermoelectric materials was focused on the development of these concepts and on their experimental proof-of-concept verification. This approach has proved to be of great value to present research directions where composite materials are being specially designed and synthesized for superior thermoelectric performance. The quantities S, σ, and κ for conventional bulk crystalline systems (3-dimensional) are interrelated in such a way that it is very difficult to control these variables independently so that ZT could be increased. This is because an increase in S (by lowering carrier concentration) usually results in a decrease in σ, and an increase in σ produces an increase in the electronic contribution to κ, according to the Wiedemann–Franz law. However, if the dimensionality of the material is decreased, the new variable of length scale becomes available for the control of materials properties. It is possible to induce dramatic change in the density of electronic states, allowing new opportunities to vary S, σ, and κ quasi-independently when the length scale is small enough to give rise to quantum-confinement effects as the number of atoms in any direction (x, y, or z) becomes small (e.g., less than ~100). In addition, as the dimensionality is decreased from 3D crystalline solids to 2D (quantum wells) to 1D (quantum wires) and finally to 0D (quantum dots), new physical phenomena, such as metal-semiconductor transition (as demonstrated in Bi nanowire composites [19]), are also introduced and these phenomena may also create new opportunities to vary S, σ, and κ independently. Furthermore, the introduction of many interfaces, which scatter phonons more effectively than electrons, or serve to filter out the low-energy electrons at the interfacial energy barriers, allows the development of nanostructured materials with enhanced ZT, suitable for thermoelectric applications [18].

Based on the theoretical study of how low-dimensional materials such as quantum wells [15] and quantum wires [16] could be utilized to enhance ZT of a material, Harman *et al.* grew superlattices of PbTe with embedded nanodots of PbSe by molecular beam epitaxy, and these materials exhibited a very high ZT of ~1.7 and 3.5 at 300 K and around

570 K respectively [20-25]. The lattice thermal conductivity in the superlattices is as low as ~0.33 W/mK, which is a 6 times reduction from that of bulk PbTe (~2.4 W/mK). Later experiments showed that the increase in the ZT is wholly due to the reduction of the thermal conductivity and not by an enhancement of the Seebeck coefficient [26]. Venkatasubramanian *et al.* [27] prepared p-type superlattice of Bi_2Te_3-Sb_2Te_3 by molecular beam epitaxy. Compared with normal bulk materials, the thin film materials with the superlattice structure also showed very low lattice thermal conductivity leading to high ZT values of up to 2.4 at 300 K. These early works have experimentally demonstrated that it is possible to raise the ZT of materials much beyond 1 by the use of nanostructures although the understanding of the responsible mechanisms in ZT enhancement has taken quite long time.

An additional effect that could be realized by the use of low dimensional materials (like superlattices) is *electron filtering*, which would result in a concomitant increase in the Seebeck coefficient. It was Moyzhes and Nemchinsky who first proposed that increasing the power factor using potential barrier scattering may be useful not only for a film material but also for a bulk material [28]. They proposed that the formation of a structure with potential barriers in a bulk material, such as the grain-boundary structure of a film, can result in an effective filtering of electrons of energy lower than the barrier height, thus allowing only the high energy electrons to contribute to electrical current. This in turn, will increase the Seebeck coefficient, thus leading to an enhancement of the power factor. Their proposal has been theoretically supported by calculations performed by other groups [29, 30]. Following this, Zide *et al.* demonstrated an increase in the Seebeck coefficient by means of electron filtering in superlattice composite material made of $In_{0.53}Ga_{0.47}As$ with $In_{0.53}Ga_{0.28}Al_{0.19}As$ barriers [31, 32].

Thus, in the past few years, numerous avenues have been explored in search of new physical phenomena that could lead to better thermoelectric performance, and novel materials that could exhibit these new phenomena have been developed. Some recent reviews on the different approaches include Refs. [18, 33] on nanoscale thermoelectricity, Ref. [34] on thermoelectric materials with complex unit cells and Ref. [35] on the chemical problems associated with the

design of new thermoelectric materials. In the following sections, we show why nanocomposite materials are a promising new class of materials, describe the various synthesis routes being explored and highlight some of the latest achievements in developing high *ZT* nanocomposites materials.

2. Nanocomposites as Highly Efficient Thermoelectric Materials

As described in the previous section, many studies have shown that it is possible to enhance the thermoelectric performance of materials beyond what is possible in bulk materials by the use of nanostructures, either through the quantum low-dimensional effects on the change of electronic energy states, the selective filtering of low energy electrons across a barrier, or by interfacial scattering of phonons to reduce the thermal conductivity. However, these are to be considered proof-of-concept studies and significant challenges exist in applying these superlattices thin films or nanowires to commercial applications, as they are far too expensive to fabricate, can only be made in small quantities, and are difficult to make high performance devices [36]. To achieve commercial usage, new types of nanostructured materials that preserve the advantages of the low-dimensional materials including thermal conductivity reduction and potentially power factor increase, while at the same time be cost-effective and susceptible to large-scale batch production need to be developed.

Chen and co-workers studied carefully the thermal conductivity reduction mechanisms in the aforementioned high efficiency thermoelectric superlattices [37]. They found that the periodicity of superlattices is not a necessary condition for thermal conductivity reduction. The reduced thermal conductivity in superlattices comes from the sequential interface scattering of phonons rather than the coherent superposition of phonon waves [38]. This conclusion leads naturally to the idea of using nanocomposites as potentially a cheap alternative to superlattices in the quest for high *ZT* materials [18, 39]. Such nanocomposites can be in the form of nanoparticles and nanowires embedded in a host material, or mixtures of two different kinds of nanoparticles [40]. Indeed nano-inclusions for thermoelectric materials

have been attempted before [41]. For example, by the addition of BN and B_4C nanoparticles into a Si-Ge alloy, it was founded that the thermal conductivity can be reduced appreciably. Unfortunately, the inclusion also reduces the electrical conductivity and thus the net gain in *ZT* was not large. This is because the added inert particles have a large bandgap and thus introducing a high electric potential barrier that scatters electrons. This indicates that one should carefully choose the materials with matched electronic properties. Recent experimental results [23, 27] show no significant reduction in the electrical conductivity was observed for current flow perpendicular to the interface of Bi_2Te_3/Sb_2Te_3 superlattices and along the interface of PbTe/PbSeTe quantum-dot superlattices. This demonstrates that by properly choosing the mismatch in electronic properties, the electron transport properties can be maintained at a level comparable to bulk materials or even enhanced using interfaces as energy filters or energy quantization barriers. At the present time a number of research groups are developing nanocomposite materials with a potential for scale-up and practical applications. Section 4 highlights some of recent achievements. The overarching goals for designing these nanocomposites materials are to introduce many interfaces that are specially chosen to: 1) reduce the thermal conductivity more than the electrical conductivity conduction by interface scattering, and 2) to increase Seebeck coefficient (for example, by carrier-energy filtering or by quantum confinement) more than decreasing the electrical conductivity, thereby yielding an increase in power factor, with both goals helping to increase *ZT*.

Nanocomposite materials offer a promising approach for the preparation of bulk samples with nanostructured constituents. As reviewed in Sec. 3, a variety of materials synthesis processes and approaches have been suggested by various research groups, involving different materials systems and processing methods, utilizing a number of common fundamental concepts. Such nanocomposites can be easily handled for both material property measurements and characterization; they can also be assembled into a variety of shapes for device applications, and can be scaled up for commercial applications. The question is can nanocomposites replicate the enhancements obtained in samples made by atomically precise methods such as molecular beam

expitaxy grown superlattices? Based on an effective medium theory they developed, Bergman and Levy [42] showed that figure of merit of a composite of two materials A and B can never exceed the highest of either A or B (though the power factor can [43]). Nevertheless, in view of the fact that this theory was based on a phenomenological description without the details of the transport mechanisms, it is conceivable that composites made with nanoscale structures that influence the electron and phonon transport in different ways than bulk composites will show better thermoelectric performance. In the past, some theoretical and modeling studies have been attempted to investigate phonon and electron transport in low dimensional structures such as superlattices and nanocomposites. In the following, we describe some of the modeling studies that have been performed in the recent past to study the effect of nanostructures on thermal and electrical transport in nanocomposites. In Sec. 4, we will describe a selected number of recent developments that have taken place in the recent past with emphasis on advances made since the last review in the subject was written [18].

2.1. Modeling of Phonon Transport

Considering that the phonon wavelength for dominant phonon heat carriers is about 1 nm and the phonon mean free path could be in the order of 100 nm [44] and thermoelectric nanocomposites often are made of nanoparticles or nanowires with a characteristic length in tens of nanometers, there would be significant challenges in modeling phonon transport using electron or phonon wave mechanics while the effective medium theory based on Fourier heat conductivity is not valid. To study the thermal conductivity of thermoelectric nanocomposites, Yang and Chen heavily relied on statistical mechanics description of thermal transport and developed deterministic solution of phonon Boltzmann equation to study periodic two-dimensional nanowire composites [45, 46], and Monte Carlo simulation of phonon transport for the thermal conductivity in periodic and random (3D) nanoparticle composites [47]. Following assumptions are made for their modeling studies: (1) The phonon wave effect can be excluded. (2) The frequency-dependent

scattering rate in the bulk medium is approximated by an average phonon mean free path. (3) The interface scattering is diffuse.

It can be a daunting problem to model or to simulate the transport properties of nanocomposites since the distribution of the nanoparticle size and location can vary a lot. To accurately model the transport, the simulation domain should be as large as possible, or even the same size as the sample. The memory and computational time requirements for such a multiscale problem are very demanding. Simulation of the properties of a periodic structure often gives physical insights of materials even in their random form. Instead of treating the whole structure, Yang and Chen [40, 46, 47] simplified the problem by dealing with periodic nanocomposites that can be constructed by a periodic stack of a unit cell. A unit cell might consist of one nanoparticle/nanowire or many nanoparticles and nanowires. If the unit cell consists of only one nanoparticle or one nanowire, the repeating structure is a simple stack of a periodic nanocomposite. If the unit cell consists of many nanoparticles and nanowires inside and the distribution inside the unit cell (simulation box) is random, the nanocomposite is then semi-periodic, i.e, long range periodic but random inside the unit cell.

The study shows that the prevailing approach to model thermal conductivity of nanocomposites, which includes the interface thermal resistance, or Kapitza resistance, with the Fourier heat conduction theory, underpredicts the effect of interface for thermal conductivity reduction since the Fourier heat conduction theory is based on the diffusion picture and is not applicable when the phonon mean free path is longer than the characteristic length of the nanocomposites such as the particle diameter and/or interparticle separation distance.

Figure 5 shows the size effect on the thermal conductivity of Si_{1-x}-Ge_x nanocomposites with Si nanoparticles embedded in Ge matrix. First of all, for fixed size of silicon nanoparticles, the less the atomic percentage of germanium, which has lower thermal conductivity than silicon, the lower is the effective thermal conductivity of the nanocomposites. This is very different from macroscale composites, in which the effective thermal conductivity increases with the decreasing volumetric fraction of the lower thermal conductivity component. This is caused by the ballistic transport of phonons in both the host material and

the nanoparticles, and the interface resistance between the host material and the nanowires.

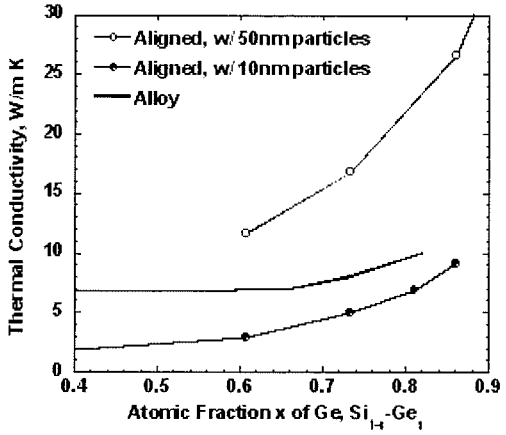

Figure 5. Size effects on the thermal conductivity of nanocomposites with Si nanoparticles embedded in Ge matrix. Reprinted with permission from Ref. [47]: M. S. Jeng, R. G. Yang, D. Song, and G. Chen, Journal of Heat Transfer-Transactions of the ASME **130**, 042410 (2008) Copyright @ American Society of Mechanical Engineers.

The comparison of the thermal conductivity of the nanocomposites with 50 nm silicon particles and 10 nm silicon particles simply aligned in germanium matrix shows that the thermal conductivity decreases as the size of the nanoparticles decreases. The comparison of thermal conductivity of nanocomposites with the corresponding alloy value also demonstrates that nanocomposite can be an effective approach to reduce the thermal conductivity and thus to develop high-efficiency thermoelectric material. Jeng *et al.* [47] also compared the thermal conductivity of periodic and random nanocomposites and found out that the randomness either in particle size or in particle location distribution causes only slight fluctuation but is not a dominant factor for thermal conductivity reduction.

Based on the fact that the phonon-interface scattering dominates the thermal conductivity reduction for nanocomposites, Yang *et al.* proposed to use interfacial area per unit volume (interface density) as a unified parameter to replace the nanoparticle/nanowire size and the atomic

composition and to correlate the wide spreading thermal conductivity data. Figure 6 shows that the thermal conductivity data of nanoparticle/nanowire composites falls nicely onto one curve as a function of interfacial area per unit volume. The randomness either in particle size or position distribution causes slight fluctuation but is not a dominant factor for thermal conductivity reduction. The key for thermal conductivity reduction is to have high interface density where nanoparticle composites can have much higher interface density than simple 1-D stacks such as those expensive periodic superlattices, thus nanocomposites benefits *ZT* enhancement in terms of thermal conductivity reduction.

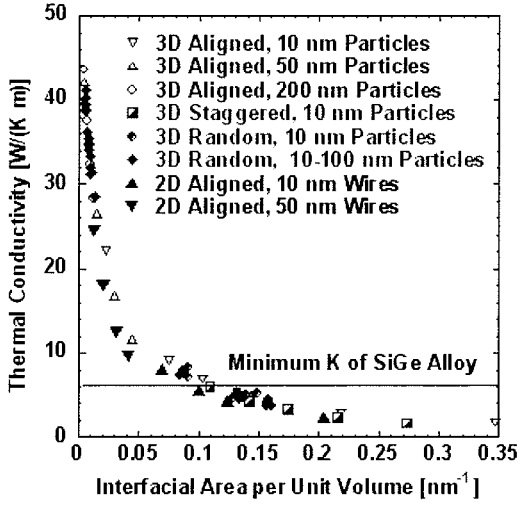

Figure 6. Thermal conductivity of nanocomposites as a function of interfacial area per unit volume (interface density). The thermal conductivity data of nanoparticle composites falls into one curve as a function of interfacial area per unit volume. At sufficiently high interface densities, the thermal conductivity of the nanocomposite reaches a value lower than that of an alloy of the same composition. Reprinted with permission from Ref. [47]: M. S. Jeng, R. G. Yang, D. Song, and G. Chen, Journal of Heat Transfer-Transactions of the ASME **130**, 042410 (2008) Copyright @ American Society of Mechanical Engineers.

Figure 7 shows the temperature-dependent thermal conductivity of nanoparticle composites. Boundary scattering results in very different temperature dependence of the thermal conductivity of nanocomposites

comparing to their bulk counterpart where at high temperature the thermal conductivity is dominated by the Umklapp phonon-phonon scattering process. The thermal conductivity of Si-Ge nanocomposites with 10 nm particles in the germanium matrix is almost temperature independent.

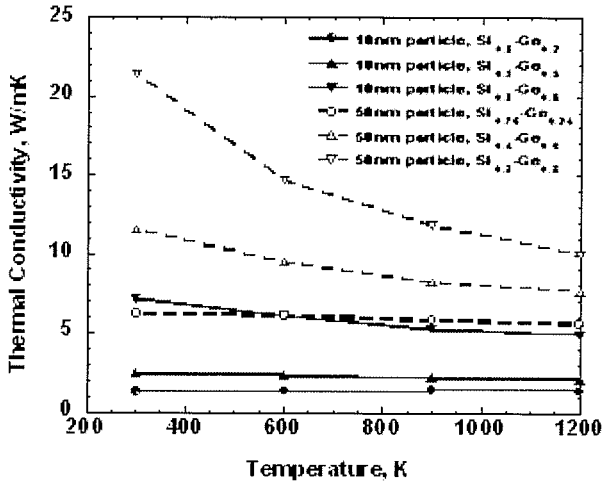

Figure 7. Temperature-dependent thermal conductivity of Si-Ge nanoparticle composites. Reprinted with permission from Ref. [47]: M. S. Jeng, R. G. Yang, D. Song, and G. Chen, Journal of Heat Transfer-Transactions of the ASME **130**, 042410 (2008) Copyright @ American Society of Mechanical Engineers.

To conclude, thermal conductivity of nanocomposites can be effectively reduced which renders nanocomposite approach as potentially a cheap alternative to superlattices for high *ZT* material development. The challenge is to properly choose the mismatch in electronic properties between the constituent materials so that the electron transport properties can be maintained or even enhanced.

2.2. Modeling of Electron Transport

The modeling tool for electron transport in nanocomposites is relatively rare. In theory, electron transport in nanocomposites can be modeled similarly to that of phonons, such as developing the Boltzmann

equation solver or Monte Carlo simulation for electron transport, as long as quantum confinement is negligible, which is often the case for random nanocomposites. However, Monte Carlo simulation of thermoelectric transport of electrons in nanocomposites is considerably more challenging because of the possibility of nonequilibrium between electrons and phonons at the interfacial region and the requirement of solving concurrently the Poisson equation to determine the electrostatic potential.

Simplified models where electron transport properties are calculated using standard Boltzmann equation expressions in the relaxation time approximation have previously been attempted [48, 49]. Yang and Chen [50] extended this model to study the thermoelectric transport properties of electrons in SiGe nanocomposites, where the nanocomposite is made by compacted SiGe alloys nanoparticles. The formulation of the transport properties are written similarly as that for bulk materials [49], which is relatively easy to implement, with an inclusion of interface scattering model.

The interface scattering can be viewed as electron energy filters [29, 51]. At the boundaries of two different grains (nanoparticles), low energy electrons are reflected and high energy electrons pass through. Thus the relaxation time due to boundary scattering can be written as,

$$\frac{1}{\tau_b} = \frac{v}{\delta} = \frac{6\sqrt{2E/m}}{d} \quad \text{when } E < E_b$$

$$\frac{1}{\tau_b} = 0 \quad \text{when } E > E_b \tag{4}$$

where d is the size of nanoparticles, E_b is the energy barrier height.

Figure 8 shows the temperature dependent electrical conductivity, Seebeck coefficient, and power factor for compacted nanoparticle composites made of $Si_{0.8}Ge_{0.2}$ alloy as a function of energy barrier height. The nanoparticle diameter is assumed to be 20 nm and the doping concentration is assumed to be 1.0×10^{20} cm^{-3}. As shown in Fig. 8(a), the electrical conductivity decreases with energy barrier height and the Seebeck coefficient increases with energy barrier height due to the low

energy carrier filtering. Figure 8(b) shows that there exists an optimum barrier height for the power factor enhancement. Overall the enhancement is effective at low temperature and becomes less effective at high temperature, which is very similar to experiment observations [52, 53].

This simplified model could be a good tool to guide the material synthesis since it predicts the dependence of thermoelectric transport properties on carrier concentration, temperature, grain (nanoparticle) size, and energy barrier height after the input parameters are optimized with experimental data.

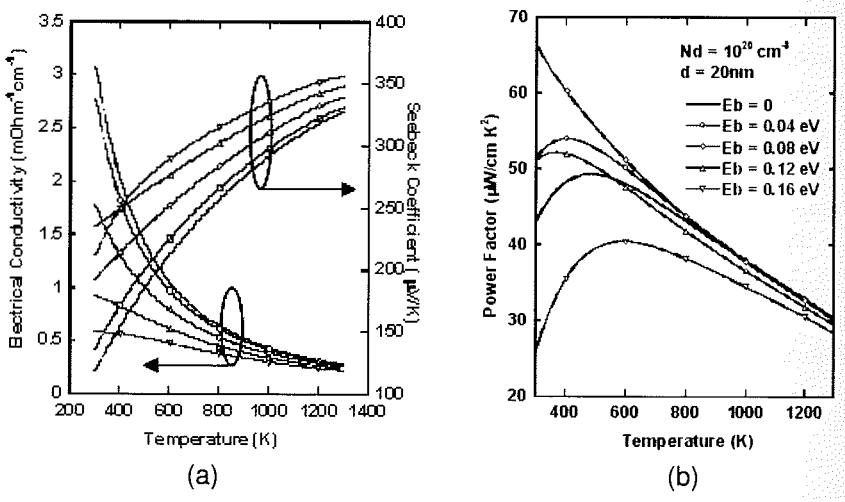

Figure 8. The temperature dependent electrical conductivity and Seebeck coefficient (a) and power factor (b) for $Si_{0.8}Ge_{0.2}$ alloy compacted nanoparticle composites as a function of energy barrier height Eb. Reprinted with permission from Ref. [50]: R. Yang and G. Chen, in *SAE World Congress* (Society of Automotive Engineers, 2006), Article # 2006-01-0289. Copyright @ Society of Automotive Engineers

Faleev and Leonard [54] developed a model for predicting the Seebeck coefficient, electrical conductivity and *ZT* of materials with nanoscale metallic inclusions, using the idea of the band bending at the metal-semiconductor interface acting as energy filters. They found that the Seebeck coefficient of the nanocomposite material is always enhanced compared to the inclusion-free system, and that the smaller the

nanoinclusion, the greater the enhancement. Similar to Yang and Chen [50], they also found that the power factor is optimized for certain values of the boundary potential. The enhancement of the *ZT* is dominated by the reduction in the lattice thermal conductivity for low carrier density, while at high carrier density the electronic contribution becomes important.

In summary, electrical and energy transport in nanostructures differs significantly from macrostructures because of classical and quantum size effects on energy carriers. Both thermal conductivity reduction and the possibility to maintain—and even enhance—the electronic power factor in nanocomposites render cost-effective random nanocomposites as a promising alternative to expensive superlattices for high *ZT* material development. The key to thermal conductivity reduction is to have high interface density where nanocomposites can have much higher interface density than simple 1D stacks such as superlattices, thus nanocomposites benefits *ZT* enhancement in terms of thermal conductivity reduction. In the meantime, the interfaces can be viewed as energy filters for electrons which allow only electrons having higher energy to pass through the barrier, and thus enhance the Seebeck coefficient. Overall there exists an optimum barrier height and nanoparticle (grain) size for the electronic power factor enhancement due to the electrical conductivity reduction at the same time.

3. Synthesis of Thermoelectric Nanocomposites

A thermoelectric nanocomposite is a composite constructed by incorporating thermoelectric nanostructures in a matrix of a bulk thermoelectric material or compacting various thermoelectric nanostructures into bulk form. Several methods for the preparation of thermoelectric nanocomposites have been exercised. These methods to obtaining bulk samples with nanoscale features can be broadly classified into two categories: (i) compaction of nanoscale constituents (nanoparticles, nanowires, etc.) into bulk samples, (ii) *in situ* precipitation of nanoscale constituents by means of phase separation. In the following, the two routes are briefly described.

3.1. Preparation of Nanocomposites by Compaction Techniques

Several different compaction techniques have been utilized in the recent past to obtain bulk thermoelectric samples from nanoscale constituents that are synthesized by an array of physical and chemical methods. The essence of all compaction techniques is to apply high pressure for densification, and often a rather high temperature to soften the material so that plastic deformation allows better filling and material flow by diffusion to remove the remaining porosity. The challenge is in achieving high density (and low porosity) without losing the nanoscale microstructure and keeping the material chemically pure.

3.1.1. Compaction Methods

Cold compaction is a process in which powder materials are compressed in a temperature range where high temperature deformation mechanics like dislocation or diffusional creep can be neglected. Cold compressing is the most important compaction method in powder metallurgy. Thus, cold sintering offers the potential for retaining the metastable nanoscale constituents. Despite this, the nanopowders may not bond very well, leading to lower carrier mobility and therefore low *ZT*.

A more common way of consolidation of nanopowders is hot pressing, where, in addition to the high pressure, moderate to high temperature is applied to the sample simultaneously. This results in a better particle-particle bonding, and higher carrier mobility in the final sample. However, it is a challenge to retain the nanometer-sized crystal grains in the final sample because the grains can grow significantly. Figure 9 shows the TEM images of nanocomposites of $Bi_xSb_{2-x}Te_3$ prepared by ball milling and hot pressing [55]. Evidently, under the right conditions hot pressing can preserve the nanostructure and lead to enhanced thermoelectric performance.

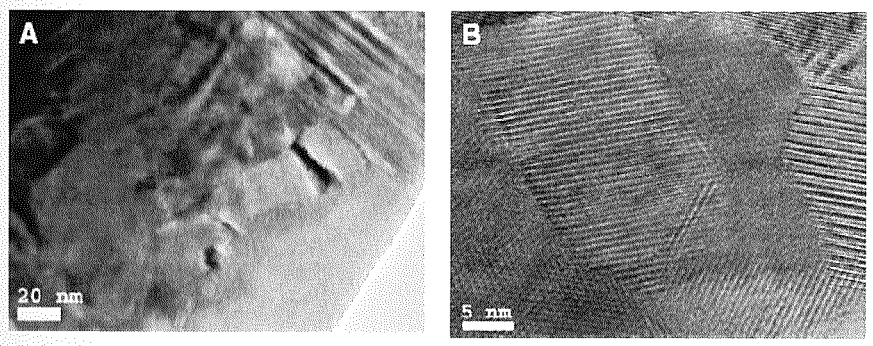

Figure 9. TEM images showing the microstructure of a hot pressed nanocomposite bulk sample of Bi-Sb-Te. (**A**) Low magnification image showing the nanograins. (**B**) High magnification image showing the nanosize, high crystallinity, random orientation and clean grain boundaries. The nanostructure is seen to be preserved even after hot pressing. Reprinted with permission from Ref. [55] B. Poudel, Q. Hao, Y. Ma, Y. Lan, A. Minnich, B. Yu, X. Yan, D. Wang, A. Muto, D. Vashaee, X. Chen, J. Liu, M. S. Dresselhaus, G. Chen, and Z. Ren, Science **320**, 634 (2008) Copyright @ American Association for the Advancement of Science.

Spark Plasma Sintering (SPS), also known as Field Assisted Sintering Technique or Pulsed Electric Current Sintering, is a novel sintering technique which is gaining increasing popularity for making thermoelectric nanocomposites [56].

In the SPS technique, the sample is heated by pulsed electric current which flows through the punch-die-sample-assembly under a low voltage. It is expected that due to the high current, at the comparatively small gaps between the powder particles, electrical discharges will occur. These discharges result in microscopic electric arcs, leading to high temperatures and pressures locally, forming a good contact between the particles. And additional advantage is that, gases and moisture that have been adsorbed on surfaces of the nanoparticles are eliminated, and oxide layers can be broken due to the arcs. Subsequently, Joule heating occurs in the compact due to the current flow, especially at spots of high electrical resistance. This temporarily overheats the sample while the overall sintering temperature is relatively low. As the heat is generated internally in the SPS, in contrast to the conventional hot pressing where the heat is provided by external heating elements, very high heating rates

(>300°C/min) and short sintering times in the range of a few minutes can be achieved resulting in a fast throughput. Also, the high speed of the process ensures it has the potential of densifying powders with nanosize or nanostructure while avoiding coarsening which accompanies standard densification routes. Densities very close to theoretical densities and excellent thermoelectric performances have been achieved in samples treated by SPS process. In view of these advantages over the other compaction methods, it is being increasingly utilized for making thermoelectric nanocomposites [57-59].

3.1.2. Synthesis of Thermoelectric Nanostructures

There are numerous techniques available to synthesize the nanoscale constituents, such as nanoparticles, nanoplates, nanowires, nanobelts and nanotubes etc. Some of the popular techniques for synthesizing thermoelectric nanostructures are described below.

Mechanical Attrition

Mechanical attrition is one of the most popular methods for synthesis of nanostructures from bulk raw materials, due not only to the convenience and minimal requirement for complex equipment, but also, to the versatility in terms of the number of different systems of materials that can be prepared this way. Mechanical attrition produces its nanostructures by the structural decomposition of coarse grains into finer structures as a result of plastic deformation and can be carried out at room temperature. The process can be performed on high energy mills, centrifugal type mill and vibratory type mill, and low energy tumbling mill. Nanoparticles, of sizes ranging from 200 nm to as low as 5-10 nm, can be prepared by the use of attritors, vibratory mills and horizontal ball mills [60]. As the process is sensitive to contamination from the milling environment, tight atmospheric control is essential to maintain the purity of the material, in particular to avoid oxidation. Consequently, an argon or nitrogen gas atmosphere is used for preparation of thermoelectric materials. Contamination from wear debris of the milling media is also a problem with mechanical attrition that may negatively impact the quality

of the alloy, requiring a judicious selection of processing time and milling speed [2]. Mechanical attrition has been used for the preparation of nanopowders of Fe-Si alloys [61], Si-Ge alloys [52, 62], PbTe [63, 64] and PbSbTe alloys[65], BiSbTe alloys [55, 66, 67], MgSiSn[68], $CoSb_3$ [69], and materials such as $La_{3-x}Te_4$ [70] that are challenging to synthesize using melt synthesis and other traditional methods.

Wet Chemistry Synthesis

Wet chemistry method is the powerful tool to generate various nanostructures in different shapes. For example, solvothermal (including hydrothermal) method synthesizes the nanostructures by using the solubility in water (or a suitable solvent) of inorganic precursors at elevated temperatures (above the critical point of the solvent) and self-formed pressures in an autoclave, and the subsequent crystallization of the dissolved material from the fluid. Compared with other synthesis routes performed at atmospheric pressure, the increased reaction temperature in the solvothermal technique may lead to an accelerated crystal growth accompanied by a narrow particle size distribution and better crystallinity. Another advantage of this method is that nanostructures of different morphologies such as nanopowders, nanorods, polygonal nanosheets, polyhedral nanoparticles and sheet-rods can be synthesized. Also, as most materials can be dissolved in the solvent by heating and pressurizing close to the critical point, this approach is suitable for synthesizing nanostructures of a wide variety of solid materials. Hydrothermal synthesis has been used to obtain nanostructures of Bi_2Te_3 [71-73], Sb_2Te_3 [74], PbX (X=S, Se, Te) [75], $CoSb_3$ [76, 77], etc. Figure 10 shows TEM images of Bi_2Te_3 nanotubes synthesized by hydrothermal processs. On the other hand, ambient solution phase method can be operated in mild conditions to fabricate different kinds of nanostructures through an anisotropic growth process by adding different surfactants or tuning reaction conditions, such as temperature, pH value etc. Bi_2Te_3 nanoplates and nanorods have been successfully fabricated using this method [78, 79], and using a two step process, Te/Bi_2Te_3 core-shell nanowires can be obtained [80]. Furthermore, rough silicon

nanowires can be synthesized through a wet etching process and were recently reported with enhanced thermoelectric performance [81].

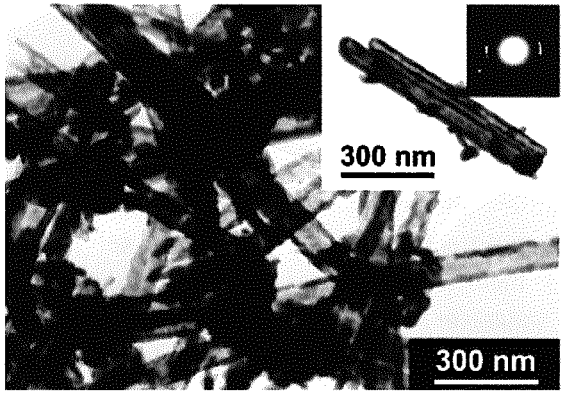

Figure 10. TEM photos of hydrothermally synthesized Bi_2Te_3 nanotubes. Reprinted with permission from Ref. [71] X. B. Zhao, X. H. Ji, Y. H. Zhang, T. J. Zhu, J. P. Tu, and X. B. Zhang, Applied Physics Letters **86**, 062111 (2005), Copyright @ American Physical Society.

Electrochemical Deposition

Electrochemical deposition provides a facile and effective route to fabricate various nanostructured metal alloys for thermoelectric applications [82, 83]. Stacy's group made a breakthrough by fabricating high quality Bi_2Te_3 nanowire arrays for the first time using the porous anodic alumina (PAA) template assisted electrodeposition process. This technique has been quickly developed as a popular method to obtain various thermoelectric nanowire arrays, such as: Bi_2Te_3, Sb_2Te_3, Bi-Sb-Te, Bi-Te-Se, $CoSb_3$, PbTe etc. [84-89].

A high degree of control in the diameter and length of the nanowires can be exercised in this method. The diameter of as-obtained nanowires ranges from 20 to 300 nm and is related to the template pore size, while the length depends on the electrodeposition time. Moreover, the alloy composition can be adjusted by changing the content of electrolyte solution [90], and the orientation of the nanowire arrays can be changed

by tuning the deposition potential or using pulsed electrodeposition process [91]. Uniformity of growth can also be achieved by electroplating in low temperature [92]. Furthermore, in some special electrodeposition conditions, novel hollow thermoelectric nanostructures can be obtained. Li *et al.* reported the successful fabrication of Bi nanotube arrays [93], and Zhu's group was able to synthesize Bi_2Te_3 and relative compounds nanotube arrays [94]. On the other hand, even without the assistance of templates, one-dimensional chinelike Bi-Sb nanostructure was fabricated through a template-free electrodeposition process by Zhou *et al.* [95], and PbTe cubes can be directly deposited on the polycrystalline gold substrate by Xiao *et al.* [96]. Using the cyclic electrodeposition/stripping method, significant amounts of long polycrystalline Bi-Te nanowires were obtained on highly oriented pyrolytic graphite (HOPG) surface [97].

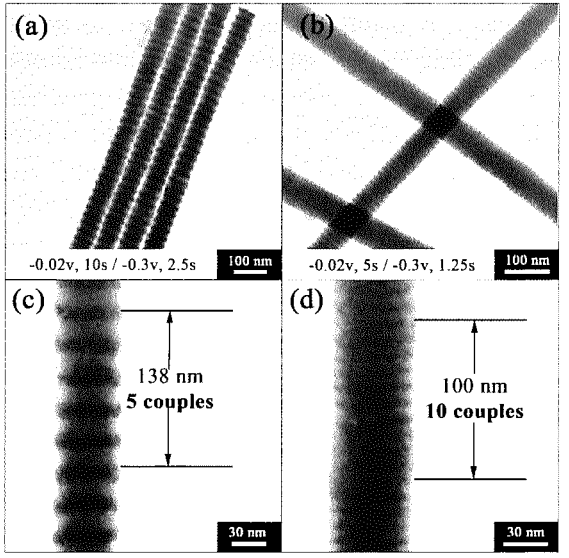

Figure 11. (a) and (b) show the TEM images of multilayered Bi_2Te_3/Sb nanowires deposited in different conditions labeled in the bottom of each corresponding figure. (c) and (d) are the corresponding high magnification TEM images. Reprinted with persmission from Ref. [100]: W. Wang, G. Q. Zhang, and X. G. Li, Journal of Physical Chemistry C **112**, 15190 (2008) Copyright @ American Chemical Society.

Electrodeposition can also be used to synthesize various heterostructured nanomaterials. Using template assisted pulsed electrodeposition, different kinds of thermoelectric materials can be deposited alternately and periodically, by applying different deposition potentials [98, 99]. Wang *et al.* reported a detailed study of Bi-Sb-Te system and successfully manipulated the growth of Bi_2Te_3/Sb heterostructure nanowires with desired period, and the minimum period of as-synthesized Bi_2Te_3/Sb heterostructure nanowires to as low as 10 nm (Fig. 11) [100]. They also fabricated Bi_2Te_3/Te heterostructured nanowire arrays through a nanoconfined precipitation process [101].

Inert Gas Condensation

Inert gas condensation is a versatile process in use today for synthesizing experimental quantities of nanostructured metallic and intermetallic powders. A feature of the process is its ability to generate non-agglomerated nanopowders, which can be sintered at relatively low temperatures. An evaporative source is used to generate the powder particles, which are convectively transported to and collected on a cold substrate. The nanoparticles develop in a thermalizing zone just above the evaporative source, due to interactions between the hot vapor species and the much colder inert gas atoms (typically 1-20 mbar pressure) in the chamber. Recently, this method has been utilized for making Si-Ge nanocomposites [102].

Sonochemical Synthesis

The underlying mechanism of sonochemistry arises from the acoustic cavitation phenomenon, that is the formation, growth and implosive collapse of bubbles in a liquid medium due to irradiation with ultrasonic waves. Extremely high temperatures (>5000 K), pressures (>20 MPa), and very high cooling rates (>10^7 K/s) can be attained locally during acoustic cavitation that lead to many unique properties in the irradiated solution [103]. The remarkable advantages of this method include a rapid reaction rate, the controllable reaction condition and the ability to form nanoparticles with uniform shapes, narrow size distributions and high

purities. Sonochemical synthesis method has been used to obtain nanocrystals of Bi_2Se_3 [104], Bi_2Te_3 and intermediate compounds [105], and other metal tellurides and selenides [106]. Figure 12 shows a TEM micrograph of Bi_2Se_3 nanocrystals made by sonochemical synthesis.

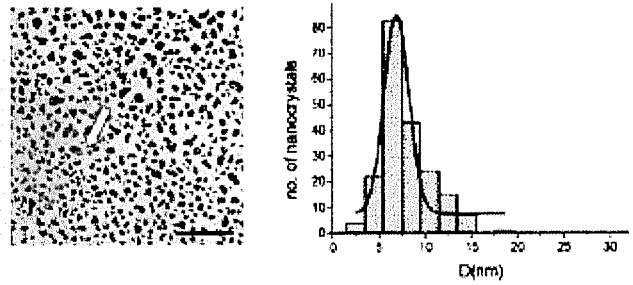

Figure 12. TEM image and a plot of the size distribution of nanocrystals of Bi_2Se_3 prepared by sonochemical synthesis. The scale of the TEM image is 100 nm. Reprinted with permission from Ref. [104] X. F. Qiu, J. J. Zhu, L. Pu, Y. Shi, Y. D. Zheng, and H. Y. Chen, Inorganic Chemistry Communications **7**, 319 (2004) Copyright @ Elsevier.

In addition to the above methods, chemical vapor deposition [107], and sol–gel process [108] have also been explored to synthesize thermoelectric nanostructures.

3.2. Synthesis of Nanocomposites by Phase Separation

The phase separation method of synthesizing nanostructures *in situ* in a bulk sample is inspired by precipitation hardening of aluminum. Basically, in this process, different kinds of metals will be heated up to the liquid phase, and then quenched to obtain a homogenous solid solution. According to the miscibility gap in the phase diagram, the as-obtained metastable solid solution will decompose into different phases A and B (or phases rich in A and B during the spinodal decomposition) after a nucleation and growth process by annealing at certain duration, and thus forms the embedded precipitates in bulk matrix. The size of the precipitates increases as the duration and the temperature of the annealing process increase [109-114]. For example, according to the pseudo-binary PbTe-Sb_2Te_3 phase diagram (Fig. 13), Ikeda *et al.* were able to produce the self-assembled lamellae PbTe and Sb_2Te_3 with

epitaxy-like interfaces by annealing the metastable $Pb_2Sb_6Te_{11}$ alloy. Such spontaneous formation of nanoscale features is desirable because it minimizes the possibility of oxidation and the introduction of other forms of impurities, which would lead to degradation of electrical performance.

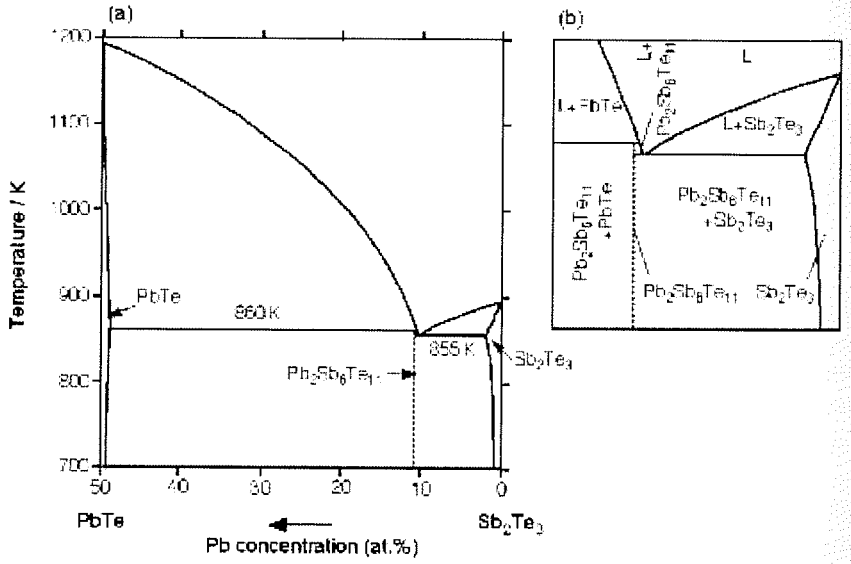

Figure 13. Pseudo-binary phase diagram of PbTe-Sb_2Te_3, with the $Pb_2Sb_6Te_{11}$ phases shown as a metastable phase. The region near the eutectic composition is enlarged in (b). Reprinted with permission from Ref. [114] : T. Ikeda, L. A. Collins, V. A. Ravi, F. S. Gascoin, S. M. Haile, and G. J. Snyder, Chemistry of Materials **19**, 763 (2007) Copyright @ American Chemical Society.

The phase separation method has also been used to obtain PbTe nanocomposites with Ag, Pb, and Sb nanoprecipitates [110, 115], $AgSbTe_2$ in PbTe [111] and in PbSnTe [112], and PbS in PbTe [113]. Figure 14(a) shows a TEM micrograph of LAST-18 sample ($AgPb_{18}SbTe_{20}$) obtained by phase separation process. The sample shows nano-sized region of the crystal structure that is Ag-Sb–rich in composition. The surrounding structure is epitaxially related to this feature, but is Ag-Sb–poor in composition, and closer to that of PbTe. Figure 14(b) shows the TEM image of the lamellar nanostructure

formed spontaneously by the separation of PbSbTe into Sb_2Te_3-rich and PbTe-rich phases.

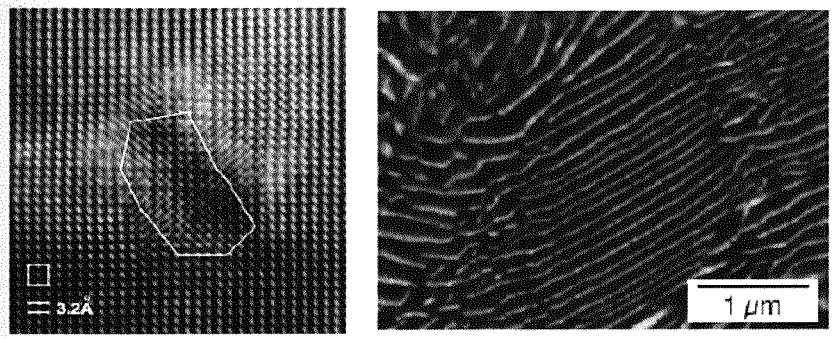

(a) (b)

Figure 14. (a) TEM image of a $AgPb_{18}SbTe_{20}$ sample showing a nano-sized region (a "nanodot" shown in the enclosed area) of the crystal structure that is Ag-Sb–rich in composition. The surrounding structure, which is epitaxially related to this feature, is Ag-Sb–poor in composition, and closer to that of PbTe. Reprinted with permission from Ref. [111] : K. F. Hsu, *et al.* Science 303, 818 (2004) Copyright @ American Association for the Advancement of Science. (b) Microstructure of metastable phase $Pb_2Sb_6Te_{11}$ transformed into self-assembled lamellae of Sb_2Te_3 and PbTe regions by annealing. The lighter regions are PbTe, and the darker regions are Sb_2Te. Reprinted with permission from Ref. [114] : T. Ikeda, L. A. Collins, V. A. Ravi, F. S. Gascoin, S. M. Haile, and G. J. Snyder, Chemistry of Materials **19**, 763 (2007) Copyright @ American Chemical Society.

4. Recent Achievements in Thermoelectric Nanocomposites

As the Seebeck coefficient, the electrical conductivity and thermal conductivity are strongly temperature dependent, any thermoelectric material is suitable for operation over a limited temperature range. Corresponding to the conventional bulk thermoelectric materials as shown in Fig. 2, nanostructured bulk thermoelectric materials with enhanced *ZT* have been developed over the past 5-10 years. Figure 15 summarizes some nanostructured bulk thermoelectric materials appropriated for different temperature ranges.

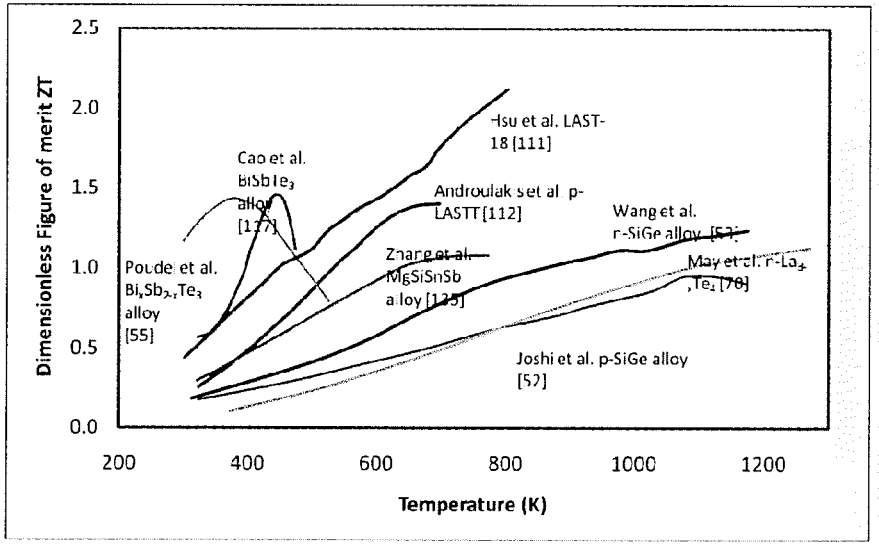

Figure 15. Plots showing the temperature dependence of the dimensionless figure of merit *ZT* of several nanocomposite materials. In comparison with Fig. 2, it may be noted that that many of the nanocomposites show enhanced *ZT*s significantly higher than 1.

4.1. Bi_2Te_3-Based Nanocomposites for Low Temperature Applications

Thermoelectric materials that operate in the range 200 K to 400 K are considered as low temperature materials. The primary application of these materials is refrigeration and temperature control of laboratory instruments. Another application of materials that operate at this temperature range lies in the recovery of low-quality waste heat from automobile radiators (~400 K) or even from electronic chips.

Currently, most of the thermoelectric devices commercially available and commonly used for applications around room temperature are based on Bi_2Te_3-Sb_2Te_3 alloys, due to the fact they have the highest *ZT* (~1) among any bulk materials around room temperature. However, the temperature range over which these devices can efficiently operate is rather small (-20°C to 100°C) due to the fast deterioration of thermoelectric properties with variation of temperature. Recently, Poudel

et al. [55] made nanostructured samples of $Bi_xSb_{2-x}Te_3$ by hot pressing nanopowders obtained by ball milling of crystalline ingots of Bi_2Te_3 and Sb_2Te_3 under inert conditions. Figure 9 shows the micrograph of a sample obtained using TEM. Nanoscale crystalline features, randomly oriented with each other can be clearly seen. As shown in Fig. 15, *ZT* of about 1.2 has been reached at room temperature, and as high as 0.8 at 250°C. Comparing this data with the *ZT* of bulk $Bi_xSb_{2-x}Te_3$ materials shown in Fig. 2, it can be seen that the nanocomposite has extended the operational range of the material to a considerable extent, making it useful for both cooling and power generation applications. The high *ZT* is the result of low lattice thermal conductivity, due to the increased phonon scattering with the interfaces of nanostructures and dislocations. The nanocomposites also show a comparable or higher power factor throughout the temperature range than the bulk ingots. These samples do not suffer from cleavage problem that is common in ingots prepared by traditional zone-melting, which leads to easier device fabrication and integration.

Alternative to starting from the alloyed crystalline ingots of $Bi_xSb_{2-x}Te_3$ as in Poudel's work, nanocomposites could also be made by starting from elemental chunks of Bi, Sb and Te, which are ball milled to get nanopowders [116]. These nanopowders are then hot pressed to obtain samples that show similarly high *ZT*. The direct route from elements to nanostructured alloy-compounds is more cost-effective and environmentally friendly. The *ZT* obtained by this method are only about 10% lower than those obtained by using the compounds of Bi_2Te_3 and Sb_2Te_3 as the starting materials, apparently due to some microstructural differences and absence of minority elements like Zn, Cd.

Hydrothermal method has also been used to synthesize Bi_2Te_3 nanocomposites [73, 117-119]. Ni *et al.* synthesized nanopowders of Bi_2Te_3 using this method, which were then hot pressed with zone-melted alloy in a 10:90 ratio [73]. It was found that the nanosized powders reduce the thermal conductivity much stronger than the electrical conductivity, which results in an enhanced thermoelectric figure of merit of a nanocomposite. *ZT* value of up to 0.83 has been obtained. Further improvement on the figure of merit of the nanocomposites should be

possible by appropriate doping of the nanopowders and optimization the composition of the base alloys. Cao *et al.* [117] synthesized nanosized binary Bi_2Te_3 and Sb_2Te_3 powders by hydrothermal route, which were then hot pressed in 1:1, 1:3 and 1:7 ratios. TEM images show that the composites have a laminated structure composed of Bi_2Te_3 and Sb_2Te_3 nanolayers with the thickness varying alternately between 5 and 50 nm. The nanoscale laminated structure improves the thermoelectric performance in comparison with bulk samples of similar compositions, reaching a high *ZT* of 1.47 at 450 K for the nanocomposite of 1:1 composition. Tang *et al.* prepared bulk *p*-type Bi_2Te_3 materials with layered nanostructures combining melt spinning with spark plasma sintering [120]. The lattice thermal conductivity measured was up to 60% lower than zone melt ingot, and *ZT* is enhanced up to 70%. Figure 16 shows the lattice thermal conductivity and electrical conductivity of these samples. While the lattice thermal conductivity of all the SPS samples was lower than that of the ingot, one of the samples showed a higher electrical conductivity than the ingot, resulting in the highest *ZT* of about 1.35 at 300 K.

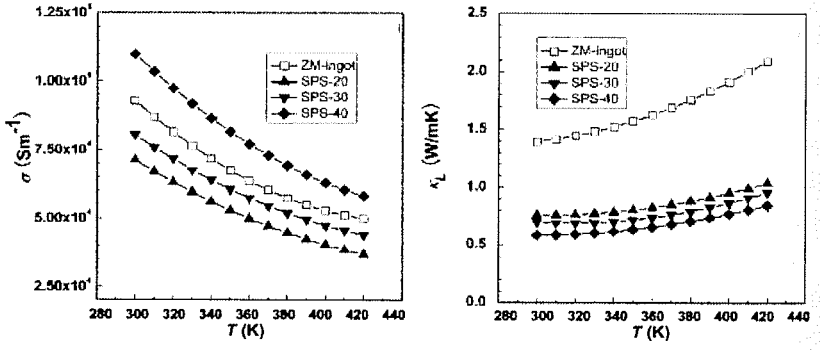

Figure 16. Electrical conductivity and thermal conductivity of layered nanostructure of Bi_2Te_3 using melt spinning combined with spark plasma sintering, in comparison with the zone melt ingot. The numbers in the sample name indicate the speed of the roller during the melt spin process in m/s. Reprinted with permission from Ref. [120] X. Tang, W. Xie, H. Li, W. Zhao, Q. Zhang and M. Niino, Appl. Phys. Lett. 90, 012102, (2007) Copyright @ American Physical Society.

Theoretical studies briefly reviewed in Sec. 2 show that nanostructuring of a bulk material can lead to up to an order of magnitude decrease in the lattice thermal conductivity, as seen in Si-Ge material system for instance. However, in Bi_2Te_3 thin films, the lattice thermal conductivity could only be reduced by a factor of 2 with respect to bulk at room temperature. The reason is likely due to the presence of structural modulations (natural nanostructures) and dislocations in bulk Bi_2Te_3 which already reduce the lattice thermal conductivity [121], and make the effect of further scattering of phonons less pronounced.

4.2. Medium Temperature Materials

Several nanocomposites materials with high *ZT* in the medium temperature range (400 K to 800 K) have been discovered. These materials could have significant impacts in waste heat recovery for both transportation sectors and industrial exhaust heat. The most prominent ones are based on alloys of PbTe, Mg_2Si, skutterudites, etc.

4.2.1. Pbte-Based Nanocomposites

Heremans *et al.* [122] prepared PbTe nanopowders by ball-milling, and then sintered the powders into bulk samples. The nanocomposites showed a slight increase in the Seebeck coefficient over bulk PbTe of the same carrier concentration. It was also found that the scattering parameter showed a slight increase as well, implying the possibility that the nanostructure was responsible for electron energy filtering. In a separate study [110], bulk PbTe samples were prepared in which nanoparticles of excess Pb or Ag metal were precipitated within the PbTe matrix by a tempering anneal process. These samples showed a remarkable enhancement (by up to 100%) in the Seebeck coefficient, and a simultaneous increase in the scattering parameter (which went from < 1 for bulk to about 3-4 in the nanoprecipitates samples). Though the origin of this increase in the scattering parameter is not clear, the effect probably is energy filtering of the electrons, resulting in the high Seebeck coefficient. On the other hand, because the mobility of the

electrons was too low, no increase in the power factor and *ZT* was obtained. More recently, Sootsman *et al.* [115] prepared PbTe with nanoprecipitates of both Pb and Sb simultaneously. This resulted in large enhancement in the power factor over that of bulk PbTe. Remarkably, and rather inexplicably, when the concentration of Sb was 3% and Pb was 2% in the nanocomposite, the electron mobility actually increased with temperature (between 300 K and 450 K). Thought ionic impurity scattering can result in a rising mobility, it is not expected to be dominant at these temperatures. Moreover, simple nanostructuring with either Pb or Sb did not result in the enhancement. Thus, co-nanostructuring seems to result in a novel effect that could probably be extended to other material systems.

Some of the highest values of the figure of merit in the medium temperature range have been obtained in the $AgSbTe_2$-$(PbTe)_m$ (LAST-m) family of thermoelectric materials [111]. These materials have NaCl structure, with the tellurium occupying the Cl positions, and silver, lead and antimony occupying the Na positions. Thus the anions carry a net charge of -2, while each of the cations carries a net charge of +2. (One pair of Ag^+ and Sb^{3+} may be considered to iso-electronically substitute for two Pb^{2+} ions in the lattice). Originally, the LAST compounds were considered to be solid solutions of $AgSbTe_2$ and PbTe. Although, according to X-ray diffraction data such as shown in Fig. 17, bulk $Ag_{1-x}Pb_mSbTe_{m+2}$ specimens with m from 6 to 18 are single-phase, the results of electron diffraction and HRTEM suggest that different microscopic phases co-exist in these specimens [123], which differ in composition. It is always found that a minority phase rich in Ag and Sb is endotaxially embedded in the majority phase poor in Ag and Sb (and rich in Pb). Thus, contrary to the previous understanding [124], $AgSbTe_2$-PbTe do not form solid solutions but exhibit extensive nanostructures caused by compositions fluctuations.

High *ZT* in the order of 2 or more has been demonstrated in the LAST materials at high temperatures. This enhancement of the figure of merit is the result of a very low lattice thermal conductivity, without much loss in the Seebeck coefficient and electrical conductivity. The spontaneously developed nanoscale inhomogeneities act as embedded nanoparticles that scatter phonons, thus reducing the lattice thermal

conductivity. The low lattice thermal conductivity is caused by the increased phonon scattering due to the distribution of three types of atoms with different masses over the lattice positions of one kind. For different m, the compounds $AgPb_mSbTe_{m+2}$ demonstrated close values of thermal conductivity, namely, below 0.5 W/mK at 700 K and 1.3 W/mK at room temperature. All compounds of the LAST family exhibit semiconductor properties with a narrow band gap of ~0.25 eV. The electrical conductivity of compounds increases with an increase in m (i.e. the PbTe content), and reaches a maximum at m=18. The LAST materials demonstrated are *n*-type. Electrons are the predominant charge carriers; hence, the Seebeck coefficient is negative. However *p*-type materials can be obtained by use for Na in place of Ag [125], or by using Sn in addition to the Ag, Pb, Sb and Te [112, 126].

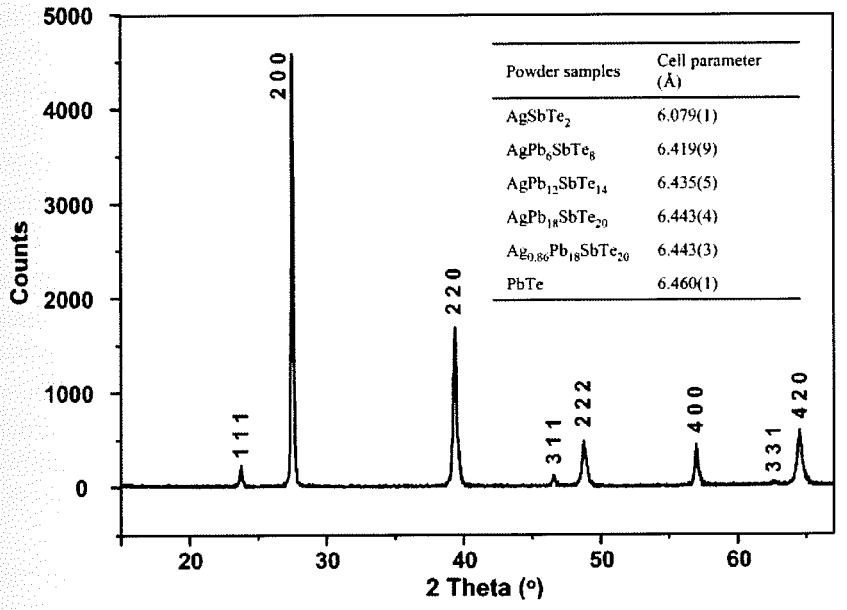

Figure 17. Typical powder X-ray diffraction pattern obtained for LAST-m samples showing a single phase rock salt-like lattice structure. However, according to electron diffraction and HRTEM, depending upon m and the processing conditions, both nanophase separation and long-range atomic ordering within the nanophases exist. From Ref. [123]: E. Quarez, K. F. Hsu, R. Pcionek, N. Frangis, E. K. Polychroniadis, and M. G. Kanatzidis, Journal of the American Chemical Society **127**, 9177 (2005).

Ab initio electronic structure calculations [127] show that the high power factor of the LAST compounds can be explained by the appearance of resonance states in the lower part of the conduction band and in the upper part of the valence band. Ag atoms introduce new electronic states near the top of the valence band of PbTe; isolated Sb atoms introduce resonant electronic states near the bottom of the PbTe conduction band. The Ag–Sb pairs result in an increase in the density of states right around the band gap, compared to that of pure PbTe. As a result, the Seebeck coefficient and the power factor are increased. However, it is also found that the increase in the power factor is small when compared with the values typical of pure lead telluride; hence, the good thermoelectric *ZT* values for the LAST compounds were largely due to the nanostructure-induced thermal conductivity reduction [128].

The LAST materials were originally synthesized by mixing the constituent elements, melting them and then cooling slowly to room temperature, leading to the formation of the nanoscale features by phase separation. Later works have shown that it is possible to obtain similar crystallographic structure and thermoelectric performances by using a mechanical alloying and annealing [58, 129] or preparing nanoparticles by hydrothermal synthesis and then compacting via pressure-less sintering, hot pressing and spark plasma sintering [130].

As PbS is immiscible in PbTe, it is possible to use a similar method as used for the preparation of the LAST compounds to obtain phase separated PbTe-PbS alloys. Androulakis *et al.* [113] prepared $(PbTe)_{1-x}(PbS)_x$ and $(Pb_{0.95}Sn_{0.05}Te)_{1-x}(PbS)_x$. These materails were found to contain nanoscale features rich in PbS, resulting in lattice thermal conductivity as low as ~0.4 W/mK at room temperature. As the mobility of the carriers stayed reasonably high (of the order of 100 cm^2/Vs), the *ZT* reached 1.5 at 642 K for the sample with x=0.08.

Ikeda *et al.* performed extensive microstructural studies in the immiscible PbTe-Sb_2Te_3 system. It was found that rapid solidification of off- and near-eutectic compositions yield a variety of microstructures, from dendritic to lamellar [131]. Starting with the metastable composition $Pb_2Sb_6Te_{11}$ close to the eutectic, they were able to obtain nanometer lamellar structures that resemble thin film superlattices [114, 132]. Figures 13 and 14 (b) show the pseudo-binary phase diagram of the

PbTe-Sb_2Te_3 system, and the naturally formed nanoscale multilayers, respectively. It was also shown that by adjusting the temperature and rate of the transformation process, it is possible to control the lamellar spacing.

4.2.2. Mg_2Si-Based Nanocomposites

An ideal thermoelectric material should not only have a high *ZT*, but should also be composed of elements that are abundant, non-toxic and light. That is why $Mg_2(Si,Sn)$ based materials have attracted much attention lately [133]. In fact, a reasonably high *ZT* value of ~1.1 was obtained at 800 K [134] in $MgSi_{0.4}Sn_{0.6}$ solid solutions, which is comparable to that of PbTe and filled skutterudites. Zhang *et al.* [135] undertook a microstructure study of high *ZT* $Mg_2Si_{0.4-x}Sn_{0.6}Sb_x$ alloys. The lattice thermal conductivity of these samples are about 1.5-2.1 W/mK at 300 K, as compared to 7.9 W/mK of Mg_2Si and 5.9 W/mK of Mg_2Sn. Interestingly, the samples showed *in situ* formed nanodots by phase separation, similar to that observed in the LAST materials. These naturally formed nanoscale compositional/structural modulations are believed to be responsible for the low value of thermal conductivity in these samples.

4.3. High Temperature Materials

Thermoelectric devices that operate in the temperature range of above 800 K are primarily of interest to power generation modules in probes for deep space exploration. Silicon-germanium alloys have been used for making the space-exploration generators.

4.3.1. Si-Ge Nanocomposites

Alloys of Si and Ge, which represent a solid solution Si_xGe_{1-x} are among the very few thermoelectric materials that operate at temperatures of above 1000 K. Elemental silicon and germanium are crystallized in the diamond-like structure. As a result of the rigid and symmetric crystal structure, they exhibit thermal conductivity too high to become good

thermoelectric materials (150 and 63 W/mK, respectively, at room temperature). However, their thermal conductivity can be reduced to approximately 5-10 W/mK by the formation of a solid solution alloying [136].

The chemical stability of Si_xGe_{1-x} solid solutions at high temperatures, particularly, against oxidation, and the high figure of merit (<~1) provide the prerequisites for the high-temperature (1000-1200 K) use of thermoelectric materials based on them. Recently much theoretical and experimental effort has been devoted to improving the rather modest figure of merit of Si-Ge alloys, with some success. With nanostructuring by means of ball milling, the thermal conductivity has been lowered than the bulk alloy, and the *ZT* of both *p*-type and *n*-type Si-Ge alloys have been shown to be enhanced [52, 53]. The *ZT* of *n*-type Si-Ge nanocomposite, in particular, has exceeded 1 at around 1100 K, for the first time in this system. Figure 18 shows the power factor and thermal conductivity of the $Si_{80}Ge_{20}$ nanocomposite samples prepared by ball milling and hot pressing.

4.3.2. Lanthanum Chalcogenides

Heavily doped lanthanum telluride and other rare-earth chalcogenides have been extensively studied in the past as potential thermoelectric materials due to their excellent thermal stability and high *ZT* [136]. They were made by either solid-state diffusion or by melt synthesis or a combination of both. However, the high temperature and pressure required for these synthesis processes led to inhomogeneities and a lack of stoichiometric reproducibility. Recently, $La_{3-x}Te_4$ alloys of specified composition were made by May *et al.* [70] using mechanical alloying and hot pressing. By utilizing much lower temperatures, while maintaining high diffusion rate by the use of mechanically alloyed starting elements (La and Te), they were able to obtain pure and homogeneous alloys of $La_{3-x}Te_4$. With an average crystallite size of about 20-30 nm after hot pressing, the resulting samples showed *ZT* in excess of 1.1 at 1273 K, which is comparable to the best *ZT* achieved in n-SiGe alloy.

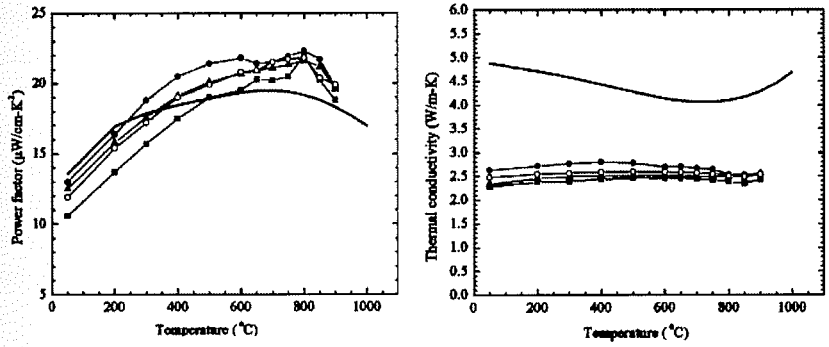

Figure 18. Temperature dependent power factor and thermal conductivity of p-type $Si_{80}Ge_{20}$ nanocomposites prepared by ball milling, hot pressing and annealing, in comparison with p-type bulk alloy used in RTGs for space missions. Reprinted with permission from Ref. [52] G. Joshi, H. Lee, Y. Lan, X. Wang, G. Zhu, D. Wang, R. W. Gould, D. C. Cuff, M. Y. Tang, M. S. Dresselhaus, G. Chen, and Z. Ren, Nano Letters **8**, 4670 (2008) Copyright @ American Chemical Society.

5. Summary

Thermoelectricity has gained much from the recent developments in nanotechnology. Thermoelectric figure of merit *ZT* has been doubled over the past 15 years from the 50-years non-changing unity to 2 and beyond after the introduction of nano-thermoelectrics. Though still not competitive with traditional mechanical energy conversion technologies, thermoelectricity could have significant impact in energy sectors, such as waste heat recovery for automobiles and solar-thermal utilization where thermal energy are free or very low cost, considering the rising demand for energy and the global warming challenges.

A few factors including quantum size effects and electron filtering for enhancing the power factor have been accounted for *ZT* enhancement in nanostructures, while most experiments show that the dominant mechanisms come from thermal conductivity reduction due to phonon-interface scattering. Careful study on thermal conductivity reduction mechanisms in nanostructures has led to the belief that nanocomposites will bring in a paradigm shift in low-cost high efficiency thermoelectric

materials search. These nanocomposites are expected to have very low thermal conductivity but maintain or even enhance the thermoelectric power factor.

Models and simulation tools for electron and phonon transport have been developed to study thermoelectric performances of nanocomposites, primary on semiconductor nanocomposites. These models could be used to qualitatively explain and provide some guidelines for nanocomposite materials design. A quantitative prediction model is highly desirable, but does not exist yet.

Various approaches have been practiced for the synthesis of nanocomposites and their constituent nanostructures with some success. Some of these methods combine the state-of-the-art nanoparticle and nanowires synthesis techniques with traditional cold and hot pressing and the recently developed spark plasma sintering. Phase-separation method has also been used to synthesize thermoelectric composites with *in situ* grown nanostructures.

For all the temperature ranges, from room temperature to 1000 K, nanocomposites with enhanced *ZT*, within a range of 1.2-2, have been successfully synthesized. The major gain in the figure of merit of these nanocomposites came from a suppression of the lattice thermal conductivity. However, most of these recent developments in nanostructured materials have focused on starting from well-known thermoelectric materials. More revolutionary ideas could be practiced using nanocomposites approach and will be needed for low-cost high efficiency thermoelectric materials.

Acknowledgments

The authors acknowledge the support from the National Science Foundation through awards CMMI 0729520 and CBET 0846521, and the Air Force Office of Scientific Research through DCT grant FA9550-08-1-0078 and MURI grant FA9550-06-1-0326. The authors also acknowledge the discussions with Professor Gang Chen and Professor Mildred Dresselhaus at MIT.

References

1. G. S. Nolas, J. Sharp, and H. J. Goldsmid, *Thermoelectrics: basic principles and new materials developments* (Springer, Berlin, New York, 2001).
2. D. M. Rowe ed., *Thermoelectrics handbook: macro to nano* (CRC/Taylor & Francis, Boca Raton, 2006).
3. A. F. Ioffe, *Semiconductor thermoelements, and Thermo-electric cooling* (Infosearch Ltd., London, 1957).
4. D. T. Morelli, T. Caillat, J. P. Fleurial, A. Borshchevsky, J. Vandersande, B. Chen, and C. Uher, Physical Review B **51**, 9622 (1995).
5. T. Caillat, A. Borshchevsky, and J. P. Fleurial, Journal of Applied Physics **80**, 4442 (1996).
6. G. S. Nolas, G. A. Slack, and S. B. Schujman, in *Recent Trends in Thermoelectric Materials Research I* (Academic Press Inc, San Diego, 2001), Vol. 69, p. 255.
7. D. M. Rowe ed., *CRC Handbook of Thermoelectrics* (CRC Press, Boca Raton, FL, 1995).
8. G. S. Nolas, D. T. Morelli, and T. M. Tritt, Annual Review of Materials Science **29**, 89 (1999).
9. B. C. Sales, D. Mandrus, and R. K. Williams, Science **272**, 1325 (1996).
10. B. C. Sales, D. Mandrus, B. C. Chakoumakos, V. Keppens, and J. R. Thompson, Physical Review B **56**, 15081 (1997).
11. G. S. Nolas, J. L. Cohn, G. A. Slack, and S. B. Schujman, Applied Physics Letters **73**, 178 (1998).
12. N. P. Blake, L. Mollnitz, G. Kresse, and H. Metiu, Journal of Chemical Physics **111**, 3133 (1999).
13. B. B. Iversen, A. E. C. Palmqvist, D. E. Cox, G. S. Nolas, G. D. Stucky, N. P. Blake, and H. Metiu, Journal of Solid State Chemistry **149**, 455 (2000).
14. S. M. Kauzlarich, S. R. Brown, and G. J. Snyder, Dalton Trans., 2099 (2007).
15. L. D. Hicks and M. S. Dresselhaus, Physical Review B **47**, 12727 (1993).
16. L. D. Hicks and M. S. Dresselhaus, Physical Review B **47**, 16631 (1993).
17. G. Chen, Physical Review B **57**, 14958 (1998).
18. M. S. Dresselhaus, G. Chen, M. Y. Tang, R. G. Yang, H. Lee, D. Z. Wang, Z. F. Ren, J. P. Fleurial, and P. Gogna, Advanced Materials **19**, 1043 (2007).
19. J. P. Heremans, C. M. Thrush, D. T. Morelli, and M. C. Wu, Physical Review Letters **88**, 216801 (2002).
20. T. C. Harman, D. L. Spears, and M. J. Manfra, Journal of Electronic Materials **25**, 1121 (1996).
21. T. C. Harman, D. L. Spears, and M. P. Walsh, Journal of Electronic Materials **28**, L1 (1999).
22. T. C. Harman, P. J. Taylor, D. L. Spears, and M. P. Walsh, Journal of Electronic Materials **29**, L1 (2000).
23. T. C. Harman, P. J. Taylor, M. P. Walsh, and B. E. LaForge, Science **297**, 2229 (2002).

24. T. C. Harman, M. P. Walsh, B. E. Laforge, and G. W. Turner, Journal of Electronic Materials **34**, L19 (2005).
25. T. C. Harman, R. E. Reeder, M. P. Walsh, B. E. LaForge, C. D. Hoyt, and G. W. Turner, Applied Physics Letters **88**, 243504 (2006).
26. C. J. Vineis, T. C. Harman, S. D. Calawa, M. P. Walsh, R. E. Reeder, R. Singh, and A. Shakouri, Physical Review B **77**, 235202 (2008).
27. R. Venkatasubramanian, E. Siivola, T. Colpitts, and B. O'Quinn, Nature **413**, 597 (2001).
28. B. Moyzhes and V. Nemchinsky, Applied Physics Letters **73**, 1895 (1998).
29. K. Nishio and T. Hirano, Japanese Journal of Applied Physics **36**, 170 (1997).
30. L. W. Whitlow and T. Hirano, Journal of Applied Physics **78**, 5460 (1995).
31. J. M. O. Zide, D. Vashaee, Z. X. Bian, G. Zeng, J. E. Bowers, A. Shakouri, and A. C. Gossard, Physical Review B **74**, 205335 (2006).
32. W. Kim, S. L. Singer, A. Majumdar, D. Vashaee, Z. Bian, A. Shakouri, G. Zeng, J. E. Bowers, J. M. O. Zide, and A. C. Gossard, Applied Physics Letters **88**, 242107 (2006).
33. J. P. Heremans, Acta Physica Polonica A **108**, 609 (2005).
34. G. J. Snyder and E. S. Toberer, Nature Materials **7**, 105 (2008).
35. A. V. Shevelkov, Uspekhi Khimii **77**, 3 (2008).
36. G. Chen, IEEE Transactions on Components and Packaging Technologies **29**, 238 (2006).
37. B. Yang and G. Chen, Physical Review B **67**, 195311 (2003).
38. G. Chen, Recent Trends in Thermoelectric Materials Research III **71**, 203 (2001).
39. R. G. Yang and G. Chen, Physical Review B **69**, 195316 (2004).
40. W. Tian and R. Yang, Journal of Applied Physics **101**, 054320 (2007).
41. N. Scoville, C. Bajgar, J. Rolfe, J. P. Fleurial, and J. Vandersande, Nanostruct Mater **5**, 207 (1995).
42. D. J. Bergman and O. Levy, Journal of Applied Physics **70**, 6821 (1991).
43. D. J. Bergman and L. G. Fel, Journal of Applied Physics **85**, 8205 (1999).
44. G. Chen, D. Borca-Tascuic, and R. G. Yang, in *Encyclopedia of Nanoscience and Nanotechnology*, edited by H. S. Nalwa (American Scientific Publishers, 2004), Vol. 7, p. 429.
45. R. G. Yang and G. Chen, Physical Review B **69** (2004).
46. R. G. Yang, G. Chen, and M. S. Dresselhaus, Physical Review B **72**, 125418 (2005).
47. M. S. Jeng, R. G. Yang, D. Song, and G. Chen, Journal of Heat Transfer-Transactions of the ASME **130**, 042410 (2008).
48. G. A. Slack and M. A. Hussain, Journal of Applied Physics 70, 2694 (1991).
49. C. B. Vining, W. Laskow, J. O. Hanson, R. R. Vanderbeck, and P. D. Gorsuch, Journal of Applied Physics 69, 4333 (1991).
50. R. Yang and G. Chen, in SAE World Congress (Society of Automotive Engineers, 2006), Article Number 2006-01-0289.

51. Y. I. Ravich, in CRC Handbook of Thermoelectrics, edited by D. M. Rowe (CRC Press, Boca Raton, FL, 1995), p. 65.
52. G. Joshi, H. Lee, Y. Lan, X. Wang, G. Zhu, D. Wang, R. W. Gould, D. C. Cuff, M. Y. Tang, M. S. Dresselhaus, G. Chen, and Z. Ren, Nano Letters **8**, 4670 (2008).
53. X. W. Wang, H. Lee, Y. C. Lan, G. H. Zhu, G. Joshi, D. Z. Wang, J. Yang, A. J. Muto, M. Y. Tang, J. Klatsky, S. Song, M. S. Dresselhaus, G. Chen, and Z. F. Ren, Applied Physics Letters **93**, 193121 (2008).
54. S. V. Faleev and F. Leonard, Physical Review B **77**, 214304 (2008).
55. B. Poudel, Q. Hao, Y. Ma, Y. Lan, A. Minnich, B. Yu, X. Yan, D. Wang, A. Muto, D. Vashaee, X. Chen, J. Liu, M. S. Dresselhaus, G. Chen, and Z. Ren, Science **320**, 634 (2008).
56. Z. A. Munir, U. Anselmi-Tamburini, and M. Ohyanagi, Journal of Materials Science **41**, 763 (2006).
57. J. Jiang, L. D. Chen, S. Q. Bai, Q. Yao, and Q. Wang, Materials Science and Engineering B-Solid State Materials for Advanced Technology **117**, 334 (2005).
58. H. Wang, J. F. Li, C. W. Nan, M. Zhou, W. S. Liu, B. P. Zhang, and T. Kita, Applied Physics Letters **88**, 092104 (2006).
59. J. Tani and H. Kido, Physica B-Condensed Matter **364**, 218 (2005).
60. A. I. Gusev and A. A. Rempel, *Nanocrystalline Materials* (Cambridge Int Science Publishing, 2004).
61. M. Umemoto, Materials Transactions JIM **36**, 373 (1995).
62. R. M. Davis and C. C. Koch, Scripta Metallurgica **21**, 305 (1987).
63. N. Bouad, R. M. Marin-Ayral, and J. C. Tedenac, Journal of Alloys and Compounds **297**, 312 (2000).
64. K. Kishimoto and T. Koyanagi, Journal of Applied Physics **92**, 2544 (2002).
65. N. Bouad, M. C. Record, J. C. Tedenac, and R. M. Marin-Ayral, Journal of Solid State Chemistry **177**, 221 (2004).
66. P. Pierrat, A. Dauscher, B. Lenoir, R. Martin-Lopez, and H. Scherrer, Journal of Materials Science **32**, 3653 (1997).
67. H. C. Kim, T. S. Oh, and D. B. Hyun, Journal of Physics and Chemistry of Solids **61**, 743 (2000).
68. J. Schilz, M. Riffel, K. Pixius, and H. J. Meyer, Powder Technology **105**, 149 (1999).
69. J. Y. Yang, Y. H. Chen, J. Y. Peng, X. L. Song, W. Zhu, J. F. Su, and R. G. Chen, Journal of Alloys and Compounds **375**, 229 (2004).
70. A. F. May, J. P. Fleurial, and G. J. Snyder, Physical Review B **78**, 125205 (2008).
71. X. B. Zhao, X. H. Ji, Y. H. Zhang, T. J. Zhu, J. P. Tu, and X. B. Zhang, Applied Physics Letters **86**, 062111 (2005).
72. N. Gothard, X. Ji, J. He, and T. M. Tritta, Journal of Applied Physics **103**, 054314 (2008).
73. H. L. Ni, X. B. Zhao, T. J. Zhu, X. H. Ji, and J. P. Tu, Journal of Alloys and Compounds **397**, 317 (2005).

74. W. Wang, W. Wang, B. Poudel, J. Yang, D. Z. Wang, and Z. F. Ren, Journal of the American Chemical Society **127**, 13792 (2005).
75. S. H. Yu, J. Yang, Y. S. Wu, Z. H. Han, J. Lu, Y. Xie, and Y. T. Qian, Journal of Materials Chemistry **8**, 1949 (1998).
76. J. L. Mi, X. B. Zhao, T. J. Zhu, J. P. Tu, and G. S. Cao, Journal of Alloys and Compounds **417**, 269 (2006).
77. J.-L. Mi, X.-B. Zhao, T.-J. Zhu, and J.-P. Tu, Journal of Inorganic Materials **23**, 715 (2008).
78. F. L. A. Purkayastha, S. Kim, T. Borca-Tasciuc, G. Ramanath, Advanced Materials **18**, 496 (2006).
79. W. Lu, Y. Ding, Y. Chen, Z. L. Wang, and J. Fang, Journal of the American Chemical Society **127**, 10112 (2005).
80. W. W. Genqiang Zhang, Xiaoguang Li, Advanced Materials **20**, 3654 (2008).
81. A. I. Hochbaum, R. K. Chen, R. D. Delgado, W. J. Liang, E. C. Garnett, M. Najarian, A. Majumdar, and P. D. Yang, Nature **451**, 163 (2008).
82. F. Xiao, C. Hangarter, B. Y. Yoo, Y. W. Rheem, K. H. Lee, and N. V. Myung, Electrochimica Acta **53**, 8103 (2008).
83. G. J. Snyder, J. R. Lim, C. K. Huang, and J. P. Fleurial, Nature Materials **2**, 528 (2003).
84. L. J. Chen, H. N. Hu, Y. X. Li, G. F. Chen, S. Y. Yu, and G. H. Wu, Chemistry Letters **35**, 170 (2006).
85. M. Martin-Gonzalez, A. L. Prieto, R. Gronsky, T. Sands, and A. M. Stacy, Advanced Materials **15**, 1003 (2003).
86. C. G. Jin, X. Q. Xiang, C. Jia, W. F. Liu, W. L. Cai, L. Z. Yao, and X. G. Li, Journal of Physical Chemistry B **108** 1844 (2004).
87. C. G. Jin, G. Q. Zhang, T. Qian, X. G. Li, and Z. Yao, Journal of Physical Chemistry B **109**, 1430 (2005).
88. M. Martin-Gonzalez, G. J. Snyder, A. L. Prieto, R. Gronsky, T. Sands, and A. M. Stacy, Nano Letters **3**, 973 (2003).
89. W. F. Liu, W. L. Cai, and L. Z. Yao, Chemistry Letters **36**, 1362 (2007).
90. W. Wang, J. F. Qu, X. L. Lu, G. Q. Zhang, G. Li, and X. G. Li, Materials Science Forum **546-549**, 2171 (2007).
91. L. Li, Y. W. Yang, X. H. Huang, G. H. Li, and L. D. Zhang, Nanotechnology **17** 1706 (2006).
92. L. Trahey, C. R. Becker, and A. M. Stacy, Nano Letters **7**, 2535 (2007).
93. L. Li, Y. W. Yang, X. H. Huang, G. H. Li, R. Ang, and L. D. Zhang, Applied Physics Letters **88** 103119 (2006).
94. X. H. Li, B. Zhou, L. Pu, and J. J. Zhu, Crystal Growth & Design **8**, 771 (2008).
95. B. Zhou, X. H. Li, and J. J. Zhu, Crystal Growth & Design **7**, 2276 (2007).
96. F. Xiao, B. Y. Yoo, K. N. Bozhilov, K. H. Lee, and N. V. Myung, Journal of Physical Chemistry C **111**, 11397 (2007).

97. E. J. Menke, Q. Li, and R. M. Penner, Nano Letters **4**, 2009 (2004).
98. F. H. Xue, G. T. Fei, B. Wu, P. Cui, and L. D. Zhang, Journal of the American Chemical Society **127** 15348 (2005).
99. B. Yoo, F. Xiao, K. N. Bozhilov, J. Herman, M. A. Ryan, and N. V. Myung, Advanced Materials **19** 296 (2007).
100. W. Wang, G. Q. Zhang, and X. G. Li, Journal of Physical Chemistry C **112**, 15190 (2008).
101. W. Wang, X. L. Lu, T. Zhang, G. Q. Zhang, W. J. Jiang, and X. G. Li, Journal of the American Chemical Society **129**, 6702 (2007).
102. M. S. Dresselhaus, G. Chen, M. Y. Tang, R. G. Yang, H. Lee, D. Z. Wang, Z. F. Ren, J. P. Fleurial, and P. Gogna, in *Materials and Technologies for direct Thermal-to-Electric Energy Conversion, MRS Symposium Proceedings*, edited by J. Yang, T. P. Hogan, R. Funahashi and G. S. Nolas, Pittsburgh, PA, 2005, Vol. 886, p. 3.
103. K. S. Suslick, Science **247**, 1439 (1990).
104. X. F. Qiu, J. J. Zhu, L. Pu, Y. Shi, Y. D. Zheng, and H. Y. Chen, Inorganic Chemistry Communications **7**, 319 (2004).
105. Y. Y. Zheng, T. J. Zhu, X. B. Zhao, J. P. Tu, and G. S. Cao, Materials Letters **59**, 2886 (2005).
106. J. P. Ge and Y. D. Li, Journal of Materials Chemistry **13**, 911 (2003).
107. B. Zhang, J. He, and T. M. Tritt, Applied Physics Letters **88**, 043119 (2006).
108. Y. Chu, X. Tang, W. Zhao, and Q. Zhang, Crystal Growth & Design **8**, 208 (2008).
109. J. P. Heremans, in *Materials and Technologies for direct Thermal-to-Electric Energy Conversion, MRS Symposium Proceedings*, edited by J. Yang, T. P. Hogan, R. Funahashi and G. S. Nolas, Pittsburgh, PA, 2005, Vol. 886, p. F04.
110. J. P. Heremans, C. M. Thrush, and D. T. Morelli, Journal of Applied Physics **98**, 063703 (2005).
111. K. F. Hsu, S. Loo, F. Guo, W. Chen, J. S. Dyck, C. Uher, T. Hogan, E. K. Polychroniadis, and M. G. Kanatzidis, Science **303**, 818 (2004).
112. J. Androulakis, K. F. Hsu, R. Pcionek, H. Kong, C. Uher, J. J. DAngelo, A. Downey, T. Hogan, and M. G. Kanatzidis, Advanced Materials **18**, 1170 (2006).
113. J. Androulakis, C. H. Lin, H. J. Kong, C. Uher, C. I. Wu, T. Hogan, B. A. Cook, T. Caillat, K. M. Paraskevopoulos, and M. G. Kanatzidis, Journal of the American Chemical Society **129**, 9780 (2007).
114. T. Ikeda, L. A. Collins, V. A. Ravi, F. S. Gascoin, S. M. Haile, and G. J. Snyder, Chemistry of Materials **19**, 763 (2007).
115. J. R. Sootsman, H. Kong, C. Uher, J. J. D'Angelo, C. I. Wu, T. P. Hogan, T. Caillat, and M. G. Kanatzidis, Angewandte Chemie-International Edition **47**, 8618 (2008).
116. Y. Ma, Q. Hao, B. Poudel, Y. C. Lan, B. Yu, D. Z. Wang, G. Chen, and Z. F. Ren, Nano Letters **8**, 2580 (2008).
117. Y. Q. Cao, X. B. Zhao, T. J. Zhu, X. B. Zhang, and J. P. Tu, Applied Physics Letters **92**, 143106 (2008).

118. X. Ji, B. Zhang, T. M. Tritt, J. W. Kolis, and A. Kumbhar, Journal of Electronic Materials **36**, 721 (2007).
119. X. H. Ji, J. He, Z. Su, N. Gothard, and T. M. Tritt, Journal of Applied Physics **104**, 034907 (2008).
120. X. F. Tang, W. J. Xie, H. Li, W. Y. Zhao, Q. J. Zhang, and M. Niino, Applied Physics Letters **90**, 012102 (2007).
121. N. Peranio, O. Eibl, and J. Nurnus, Journal of Applied Physics **100**, 114306 (2006).
122. J. P. Heremans, C. M. Thrush, and D. T. Morelli, Physical Review B **70**, 115334 (2004).
123. E. Quarez, K. F. Hsu, R. Pcionek, N. Frangis, E. K. Polychroniadis, and M. G. Kanatzidis, Journal of the American Chemical Society **127**, 9177 (2005).
124. F. D. Rosi, E. F. Hockings, and N. E. Lindenblad, RCA Review **22**, 82 (1961).
125. P. F. R. Poudeu, J. D'Angelo, A. D. Downey, J. L. Short, T. P. Hogan, and M. G. Kanatzidis, Angewandte Chemie-International Edition **45**, 3835 (2006).
126. A. Kosuga, K. Kurosaki, H. Muta, and S. Yamanaka, Journal of Alloys and Compounds **416**, 218 (2006).
127. D. Bilc, S. D. Mahanti, E. Quarez, K. F. Hsu, R. Pcionek, and M. G. Kanatzidis, Physical Review Letters **93**, 146403 (2004).
128. D. I. Bilc, S. D. Mahanti, and M. G. Kanatzidis, Physical Review B **74**, 125202 (2006).
129. M. Zhou, J. F. Li, and T. Kita, Journal of the American Chemical Society **130**, 4527 (2008).
130. K. F. Cai, C. Yan, Z. M. He, J. L. Cui, C. Stiewe, E. Müller, and H. Li, Journal of Alloys and Compounds (In Press).
131. T. Ikeda, S. M. Haile, V. A. Ravi, H. Azizgolshani, F. Gascoin, and G. J. Snyder, Acta Materialia **55**, 1227 (2007).
132. T. Ikeda, V. A. Ravi, L. A. Collins, S. M. Haile, and G. J. Snyder, Journal of Electronic Materials **36**, 716 (2007).
133. G. S. Nolas, D. Wang, and M. Beekman, Physical Review B **76**, 235204 (2007).
134. V. K. Zaitsev, M. I. Fedorov, E. A. Gurieva, I. S. Eremin, P. P. Konstantinov, A. Y. Samunin, and M. V. Vedernikov, Physical Review B **74**, 045207 (2006).
135. Q. Zhang, J. He, T. J. Zhu, S. N. Zhang, X. B. Zhao, and T. M. Tritt, Applied Physics Letters **93**, 102109 (2008).
136. C. Wood, Reports on Progress in Physics **51**, 459 (1988).